CHAPTER IV
RESULTS AND DISCUSSION

4.1 Graphite Characterization

In order to study the structure of graphite, it is vital to perform characterization studies to understand the nature of this material. Therefore, the graphite is characterized in order to relate its properties and the adsorption capacity. X-ray diffractometer, BET surface area analyzer, and Scanning Electron Microscope were applied for this purpose.

4.1.1 X-ray Diffractometer

Figure 4.1 shows X-ray diffraction pattern of the graphite with the main peak corresponding to the (002) diffraction peak.

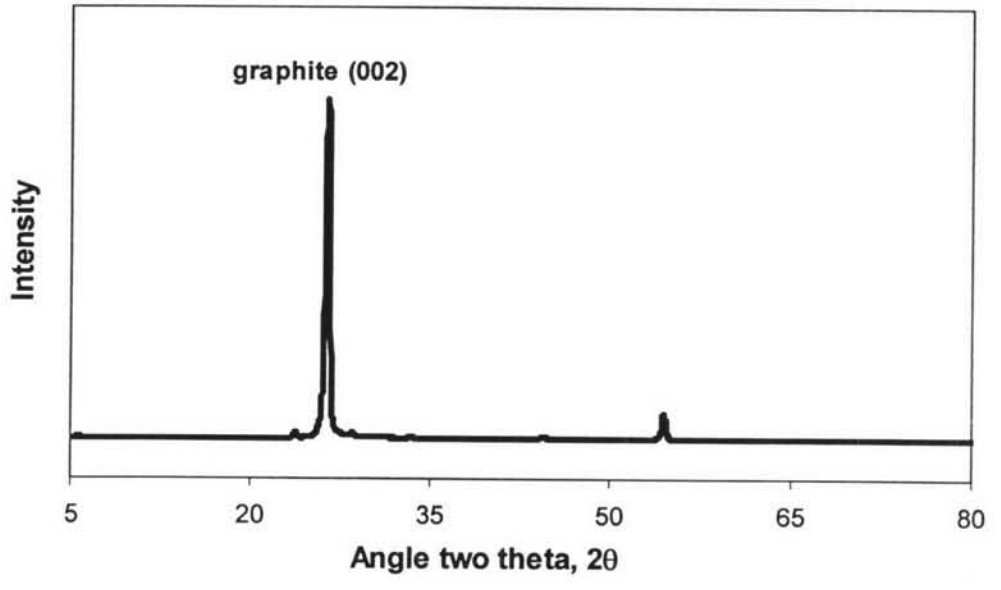

Figure 4.1 XRD profile of the studied graphite.

4.1.2 Surface Area Measurement (BET)

The specific surface area, average pore diameter, pore specific volume, and purity of graphite are shown in Table 4.1. The result shows that the

studied graphite (un-milled graphite) exhibits very low surface area, 27.6 m^2/g compared with ~1,030 m^2/g of activated carbon (Nijkamp *et al.*, 2001).

Table 4.1 Some physical properties of the studied graphite

Physical parameter	Graphite
Surface area (m^2/g)	27.6
Average pore diameter (nm)	141.87
Pore specific volume (cm^3/g)	0.13
Purity (%)	>99.99%

4.1.3 Scanning Electron Microscope

SEM image of the original graphite reveals the presence of flat sheets (graphene sheet) as shown in Figure 4.2. The figure clearly indicates that the graphite consists of multiple graphene sheets and the sheets lie on top of each layer.

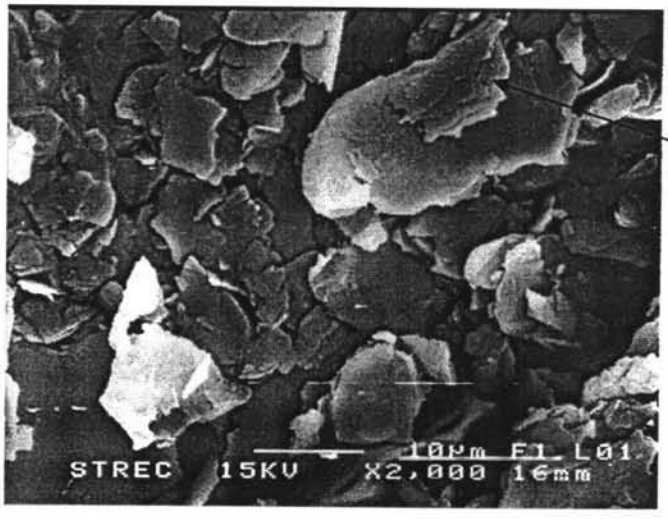

Figure 4.2 SEM image of the studied graphite.

4.2 Blank Test

It was found that when hydrogen is pressurized into the system, the hydrogen leakage is very small as shown in Figure 4.3. The result revealed that the leakage rate in the system is 9.01×10^{-6} mol/h after 80 h. With the initial hydrogen pressure at 1,600 psig, no hydrogen leakage is observed during the first 25 h. The system was adjusted to minimize the leakage so that any data correction from the hydrogen adsorption experiment is not necessary.

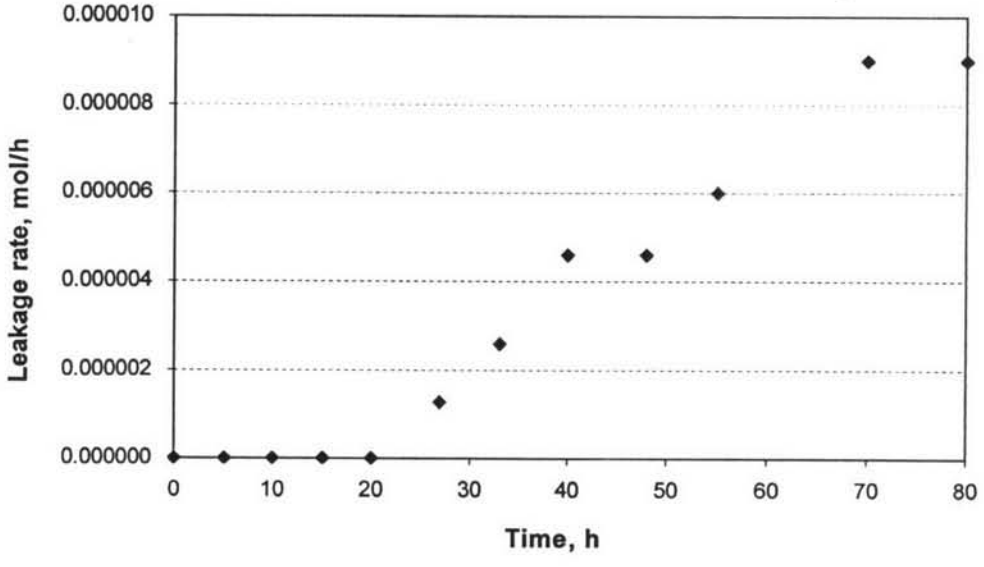

Figure 4.3 Hydrogen leakage during 80 h (initial hydrogen pressure at 1,600 psig).

4.3 Volume Calibration of the Manifold and Sample Holder

The calculated volumes of the manifold are in the range of 23.70 – 26.08 cm^3 and 28.10 – 28.88 cm^3 for the calculated dead volume of the sample holder as shown in Appendix A. The average volumes of the manifold and sample holder used in this work are 24.81 and 28.49 cm^3, respectively.

4.4 Hydrogen Adsorption

4.4.1 Effect of Milling Time

The milling process leads to the formation of nanocrystallites of graphite in two steps. The first step is pulverization perpendicular to the basal plane, and the second is pulverization parallel to the basal plane. In the first step, dangling bonds are produced and, if the milling process is carried out in hydrogen atmosphere, C-H chemical bonds will be formed (Orimo *et al.*, 2001).

In order to enhance the hydrogen uptake due to physical adsorption, it is necessary to decrease the thermal motion of hydrogen molecules on the solid surface; note that low temperatures are ideal for physical adsorption. However, this is to be anticipated that an alternative way to increase the amount of hydrogen physisorbed occurs by optimizing the morphology of the graphite. Therefore, novel materials capable of storing large amount of hydrogen should possess very high pore volume, pore diameter, and high surface area (Terres *et al.*, 2005).

The result of the milling process shows that hydrogen capacity increases with increasing milling time to 2 h (Figure 4.4), indicating the long range ordering of graphite continuously disappears (Figure 4.5). There is no diffraction peak after milling for 2 h, and there is no change in the profile for the milling time between 2 and 32 h. The increase in the hydrogen capacity corresponds to the pulverization of graphite, which forms a large amount of defective sites, leading to the increase in the hydrogen capacity (Orimo *et al.*, 1999). Nevertheless, the hydrogen capacity decreases for the milling time longer than 2 h. The result indicates that the milled graphite agglomerates during the milling process for milling time higher than 2 h (Figure 4.6). The agglomeration of graphite has an effect on the decrease in the specific surface area (Figure 4.7), resulting in the decrease in the hydrogen capacity as well. Therefore, the observation would suggest that the surface area of the milled graphite for 2 h achieves the highest hydrogen storage capacity.

Moreover, Table 4.2 shows that the milled graphite obtains the higher pore specific volume and the depressed pore diameter than un-milled graphite. The property of the depressed pore diameter appropriates for the hydrogen molecule, which hydrogen molecules have a diameter of 0.26 nm. For this reason, the pore

diameter should fit in with hydrogen molecule. Apart from this, the higher pore volume might contribute to the spread of hydrogen molecules into these pores that the milled graphite for 2 h reaches the highest hydrogen capacity may be a consequence of the suitable pore diameter and highest pore volume.

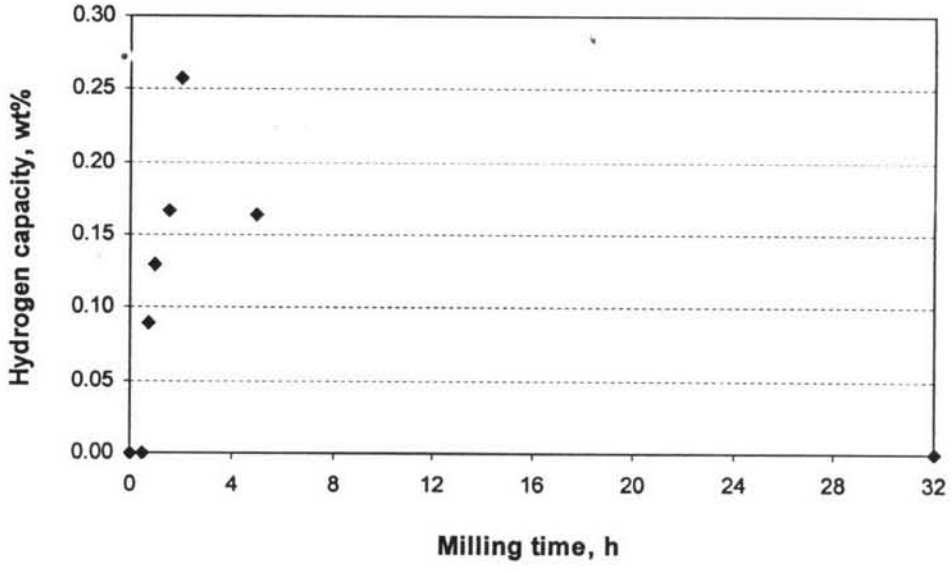

Figure 4.4 Hydrogen desorption of graphite as a function of milling time.

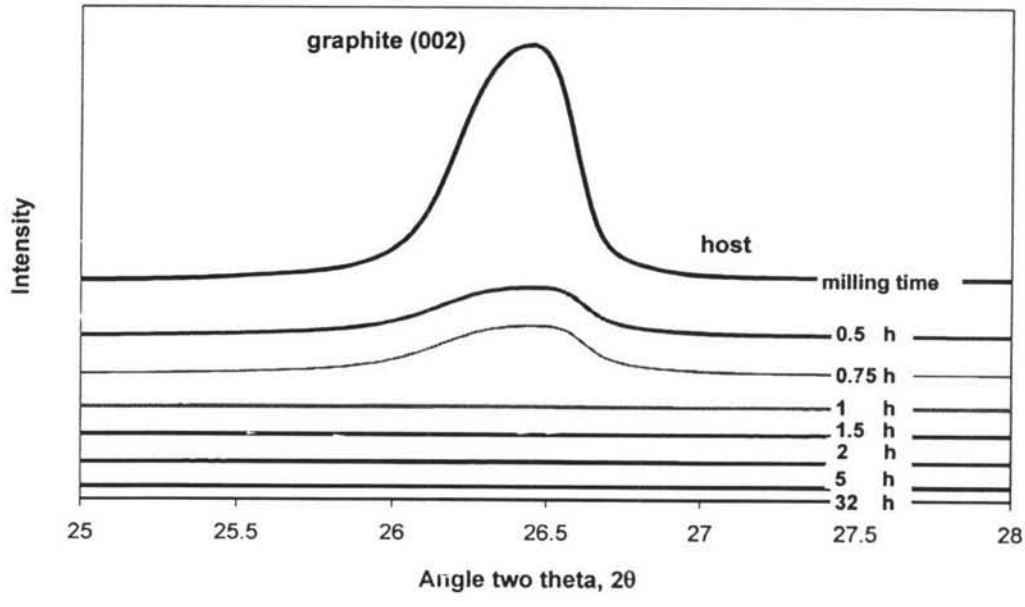

Figure 4.5 (002) diffractions of mechanically milled graphite.

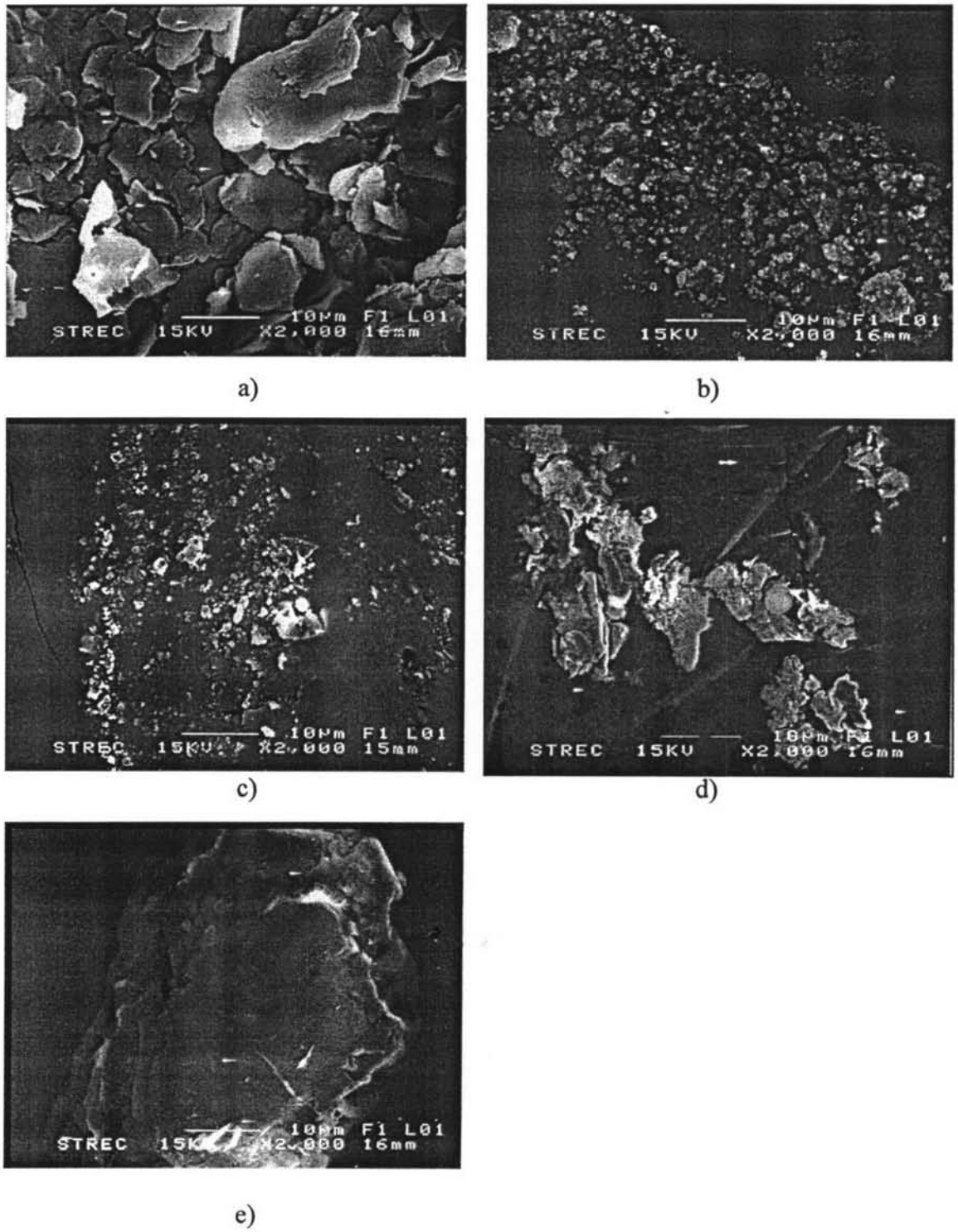

a) b) c) d) e)

Figure 4.6 SEM images of graphite: a) un-milled graphite; b) milled graphite for 1 h; c) milled graphite for 2 h; d) milled graphite for 3 h; and, e) milled graphite for 32 h.

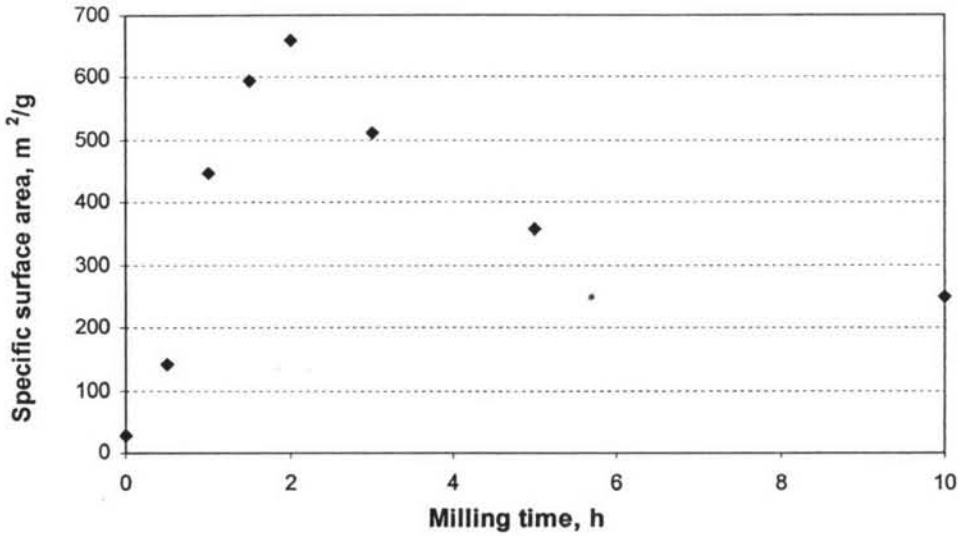

Figure 4.7 Specific surface area of the nanostructure graphite as a function of milling time.

Table 4.2 Some physical properties of the graphite, milled graphite and carbon nanotubes

Sample	Milling time (h)	Specific surface area, m^2/g	Pore specific volume, cm^3/g	Pore diameter, nm
Graphite	0	27.60	0.13	141.87
Graphite	1	447.61	0.52	8.43
Graphite	2	661.25	0.86	0.80
Graphite	3	512.06	0.65	5.62
Graphite	5	358.27	0.48	70.82
Graphite	10	248.78	0.76	221.38
Graphite	32	178.56	0.46	170.76
CNTs	1	259.38	0.90	35.15

4.4.2 Effect of Metal Loading

Graphite was modified by transition metals and by alkali earth. Iron powder, zirconium, vanadium, and titanium compounds represent the transition metals and potassium compounds as the alkali-doped on graphite by mechanically milling. The results of the samples in this work are shown in Table 4.3.

Table 4.3[*] Milling time and amount of hydrogen (determined by the volumetric method) for samples in this work

Sample	**Milling time (h)**	**Amount of H_2 (wt%)**	
		adsorption	**desorption**
Graphite	1	0.15	0.13
Graphite	2	0.29	0.26
Graphite	3	0.18	0.15
CNTs	1	0.89	0.49
Graphite + Fe (3wt%)	2	0.48	0.28
Graphite + Fe (6wt%)	2	0.32	0.10
Graphite + Fe (6wt%)	5	0.20	0.05
Graphite + Fe (3wt%)	6	0.30	0.18
Graphite + Fe (3wt%)	32	0	0
Graphite + $ZrCl_4$ (3wt%)	1	0.29	0.20
Graphite + $ZrCl_4$ (6wt%)	1	0.55	0.25
Graphite + $ZrCl_4$ (9wt%)	1	0.60	0.47
Graphite + $ZrCl_4$ (6wt%)	2	0.64	0.28
Graphite + $ZrCl_4$ (6wt%)	5	0.35	0.17
Graphite + VCl_3 (6wt%)	2	0.48	0.42
Graphite + VCl_3 (6wt%)	5	0.38	0.33
Graphite + TiO_2 (6wt%)	2	0.20	0.17
Graphite + TiO_2 (6wt%)	32	0.09	0.03
Graphite + K_2CO_3[*]	2	0.34	0.21
Graphite + K_2CO_3[*]	5	0.31	0.15

[*] K/C = 1/15

4.4.2.1 Effect of Fe on Hydrogen Storage

The result shows that Fe only slightly acts as a catalyst for the hydrogen desorption as shown in Table 4.3. In the case of 6 wt% Fe doped graphite, the amount of hydrogen is slightly desorbed owing to Fe possibly induces the hydrogen strongly adsorbs with graphite like chemisorption. Furthermore, the hydrogen capacity drastically decreases with increasing milling time due to the agglomeration of graphite during milling as shown in Figure 4.8.

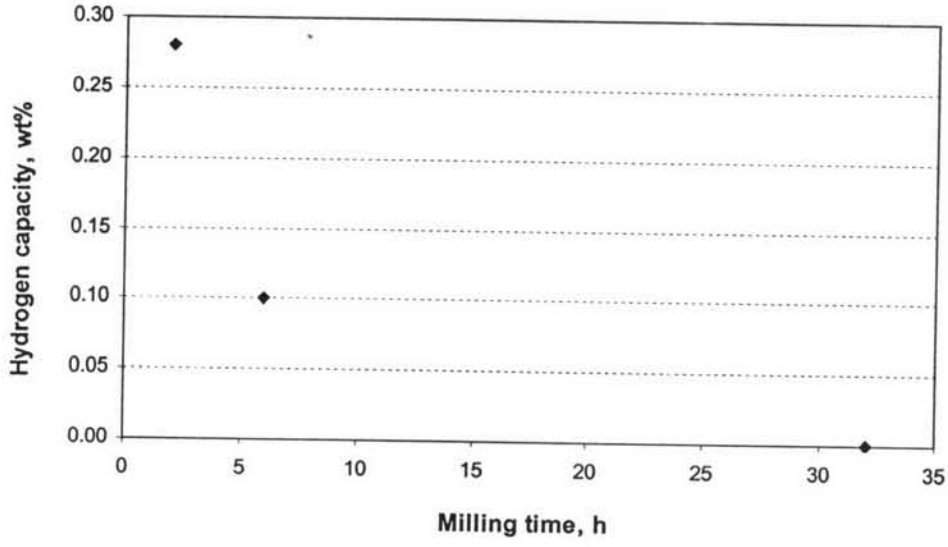

Figure 4.8 Hydrogen desorption in mechanically milled graphite doped with 3 wt% Fe.

4.4.2.2 Effect of the Amount of Zr-doped Graphite

The result shows that increasing the amount of Zr loading enhances the hydrogen capacity as shown in Figure 4.9. The 002 diffraction of graphite can be observed only from the Zr-doped graphite, whereas in the undoped graphite no diffraction peak at the same milling time could be observed, as shown in Figure 4.10. The result indicates that the crystallinity of graphite has an effect on the hydrogen uptake such that continuous structures possibly cause difficulties for hydrogen to enter the graphite. In contrast, the gaps between the graphene sheets can be paths for hydrogen to spread into the graphite. However, this does not mean that the lower crystallinities are more advantageous for hydrogen storage because the low

crystallinity may weaken the interactions between hydrogen molecules and graphite (Li *et al.*, 2001). The XRD profiles in Figure 4.10 show that the diffraction shifts to lower angle with the increase in the amount of Zr loading. The higher amount of Zr stabilizes the structure of graphite by increasing the distance between graphene sheets. This is to be anticipated that the suitable distance of graphite interlayers results in more hydrogen spreading between the graphene sheets in adsorption process. However, in the desorption process, the hydrogen released from the doped sample is higher than the undoped as shown in Figure 4.9. Furthermore, the higher amount of Zr loading leads to higher amount of hydrogen released at the same desorption temperature as can be observed in Figure 4.9. $ZrCl_4$ doped graphite first begins to release hydrogen clearly at ~80°C, and the releasing temperature is 25°C lower than the undoped sample.

In addition, 002 diffraction peaks of graphite doped with 6 wt% Zr have the same intensity compared with 9 wt% (Figure 4.10) resulting in the same distance between the graphite layers. Moreover, the hydrogen adsorption of referable samples is nearly the same as shown in Table 4.3. Therefore, graphite doped with 6 wt% metal loading would be a well condition, which can enhance the amount of hydrogen adsorption. However, the released hydrogen for graphite doped with 9 wt% Zr is higher than 6 wt%. This probably is due to the longer distance between the graphene layers can easily release hydrogen molecules.

Nevertheless, the hydrogen capacity drastically decreases with increasing milling time due to the agglomeration of graphite during the milling process.

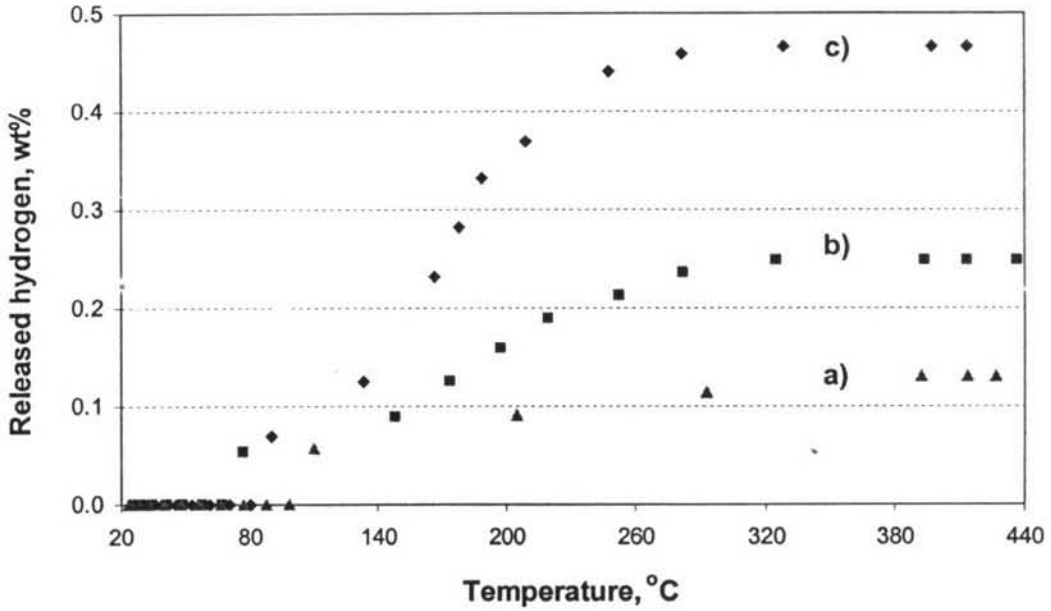

Figure 4.9 Correlation between temperature and hydrogen capacity during hydrogen desorption with the heating rate of 7.5 °C min^{-1} on milled graphite (1 h): a) undoped; b) doped with 6 wt% $ZrCl_4$; and, c) doped with 9 wt% $ZrCl_4$.

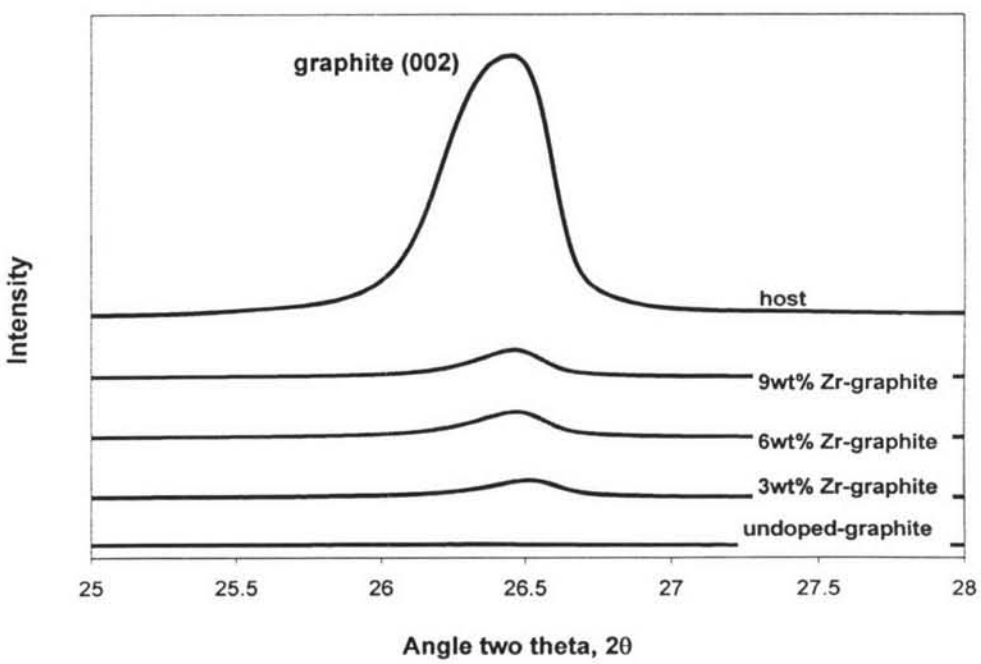

Figure 4.10 (002) diffractions of mechanically milled graphite for 1 h with various amounts of doped $ZrCl_4$.

4.4.2.3 Effect of V-doped Graphite

The property of the transition metals is confirmed by the V-doped graphite. The graph clearly indicates that 002 diffraction patterns of graphite are observed only in the V-doped graphite, which was milled for 2 and 5 h as shown in Figure 4.11. This may be attributed to the structure stability of graphite by the transition metal (Zr and V); therefore, more hydrogen probably spreads between the graphene layers, which is suitable trapping sites for hydrogen.

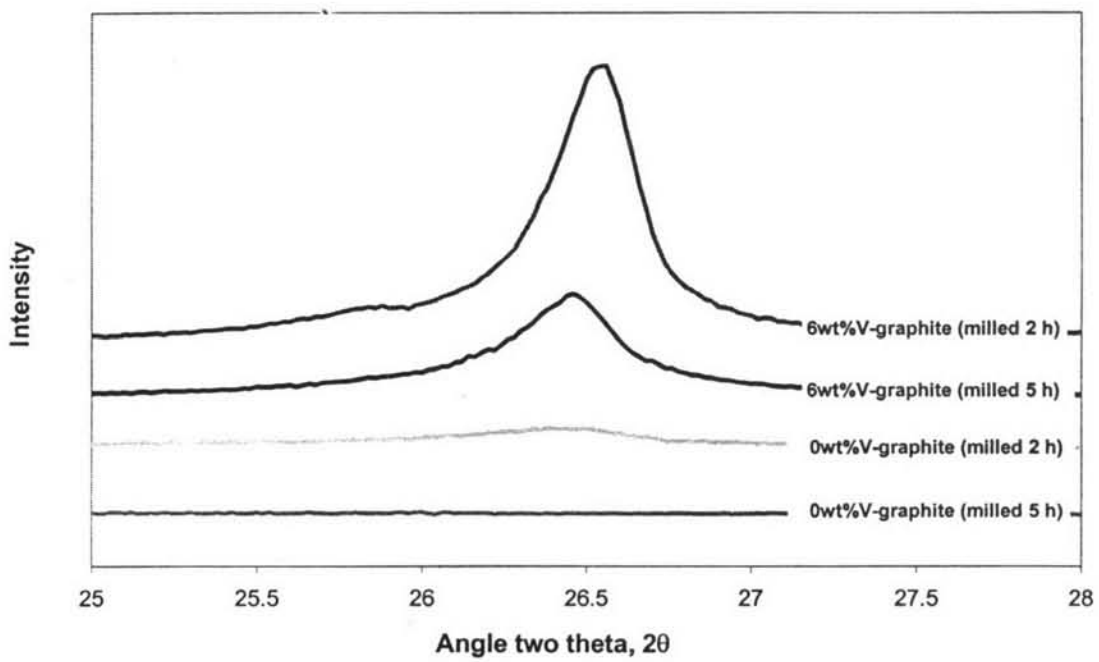

Figure 4.11 (002) diffractions of mechanically milled undoped graphite and graphite doped with 6wt%V.

4.4.2.4 Effect Ti-doped Graphite

The result shows that graphite doped with 6 wt% Ti cannot improve the hydrogen capacity compared with the undoped graphite as shown in Table 4.3. The 002 diffraction of graphite is clearly observed from the undoped graphite, whereas the Ti-doped graphite shows lower diffraction peak at the same milling time as shown in Figure 4.12. It may be suggested that TiO_2 cannot stabilize

the structure of graphite. As a result, the hydrogen molecules cannot spread between the grahene layers as the layers disappear and graphite turns to amorphous carbon.

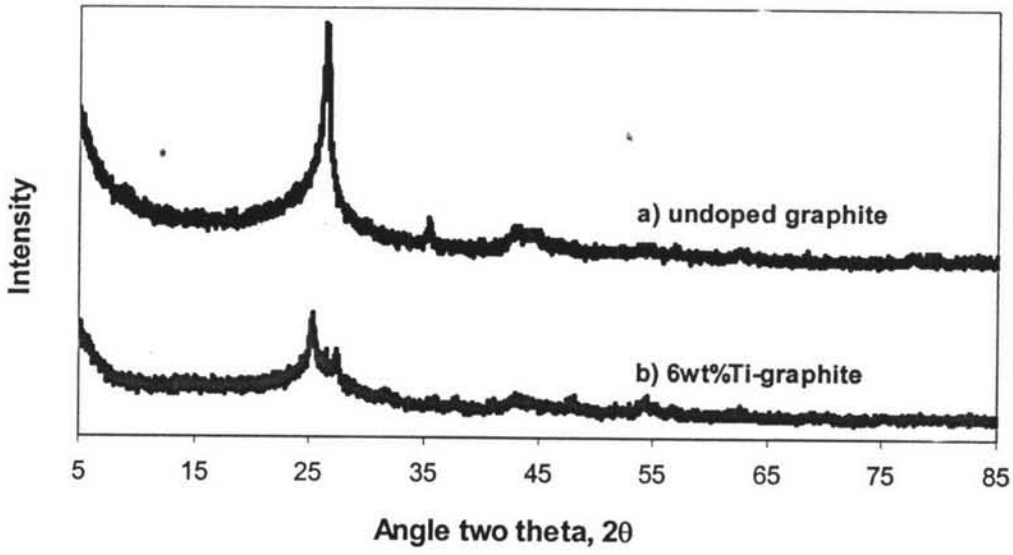

Figure 4.12 Comparison of (002) diffractions of mechanically milled graphite: a) undoped and b) doped with 6wt%Ti at the same milling time (2h).

4.4.2.5 Effect of Alkali-doped Graphite

Figure 4.13 shows that the 002 diffraction peaks of K doped graphite have the same intensity as the undoped graphite. Furthermore, the hydrogen adsorption/desorption capacity of K doped graphite is close to the undoped graphite as shown in Table 4.3. The results reveal that alkali-doped (K_2CO_3) graphite cannot improve hydrogen capacity because the crystallinity of graphite is the same as the undoped graphite. The observation suggests that not only the degree of crystallinity of graphite relates with the distance between the graphene layers, but also indicates the amount of hydrogen capacity.

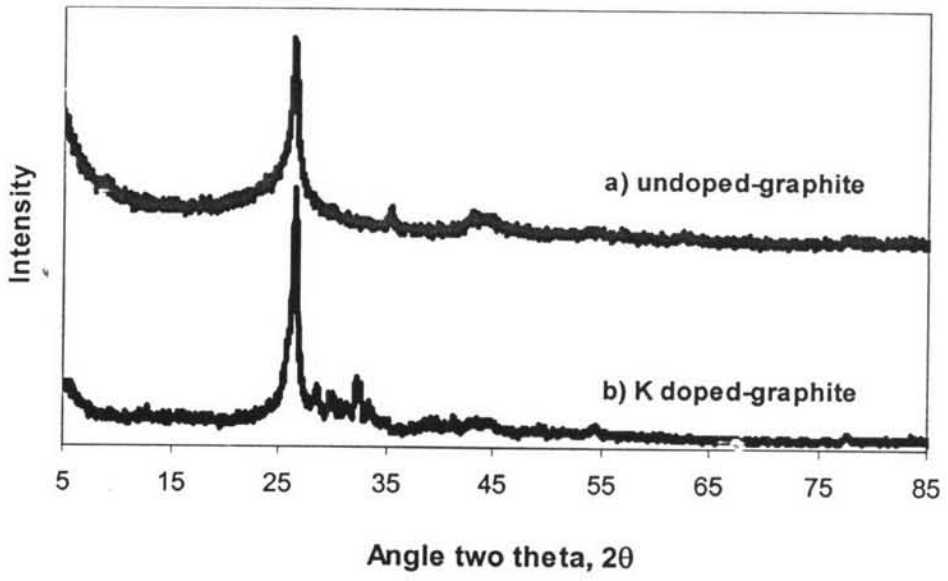

Figure 4.13 Comparison of (002) diffractions of mechanically milled graphite: a) undoped and b) doped with K_2CO_3 at the same milling time (2h).

4.4.3 Effect of Adsorbent Types

We found that carbon nanotubes adsorb 0.49 wt% H_2 and only 0.13 wt% H_2 for graphite at the same milling time (1 h). The result indicates that carbon nanotubes could store hydrogen more than graphite. This might be a consequence of larger pore volume of carbon nanotubes than graphite as shown in Table 4.2. Moreover, in the desorption process, carbon nanotubes begin to release hydrogen at 110°C as same as the graphite. However, the hydrogen released from the carbon nanotubes is higher than graphite as shown in Figure 4.14. Therefore, it may be suggested that the structure of carbon nanotubes adsorbs higher amount of hydrogen than the un-modified graphite.

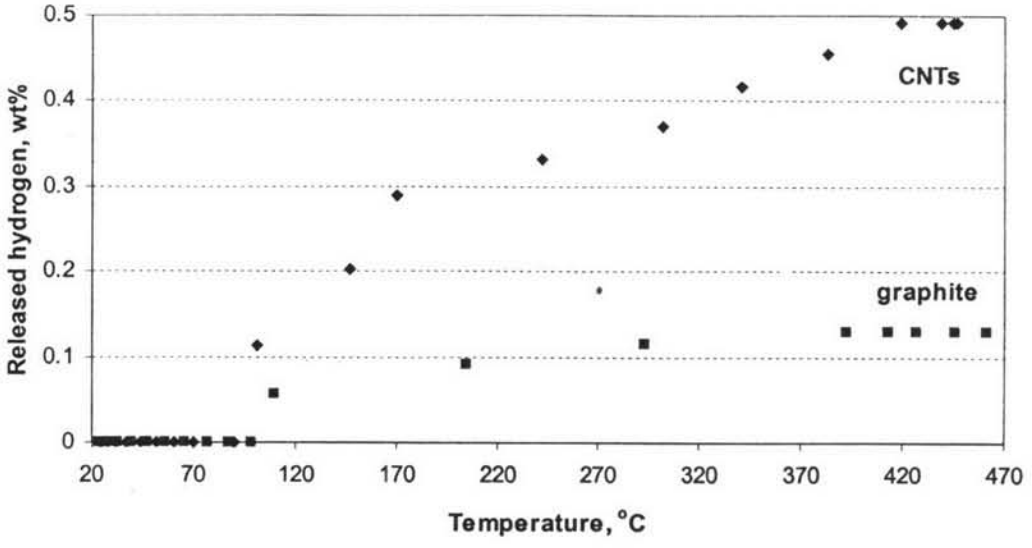

Figure 4.14 Correlation between temperature and hydrogen capacity during hydrogen desorption on carbon nanotubes and milled graphite (1 h) with the heating rate of 7.5 °C min^{-1}.